Bulletin of the Earthquake
Research Institute
Vol. 46 (1968), pp. 319-343

14. A Long Wave around a Breakwater (Case of Lateral Incidence) [IV].

By Takao Momoi,

Earthquake Research Institute.

(Read January 23, 1968.—Received January 30, 1968.)

Abstract

The long wave around the breakwater is discussed for the case of lateral incidence (incidence along the breakwater) of the invading wave. The most conspicuous feature obtained is an appearance of the reverse current (inverse for the direction of the incident wave travel) in the waters near the terminus of the leeward breakwater for very long waves.

1. Introduction

Succeeding the previous works (*Momoi*, 1967a, 1967b, and 1967c) under the same title, the long wave around the breakwater is discussed in this paper. The previous papers (*Momoi*, 1967a, 1967b and 1967c) treat long waves which invade the breakwater in a normal direction from the outer sea, while in the present article, the waves are propagated along the breakwater wings. The theory is developed by use of the method the buffer domain in a manner similar to the case of the normal incidence (*Momoi*, 1967a), though a rigorous theory is developed by using the Mathieu function (*Morse* and *Rubenstein*, 1938). The author's theory is more preferable in numerical calculation than Morse and Rubenstein's one, since the calculation of the Mathieu function is more tedious than that of the Bessel function in a computer.

2. Theory

2,1. Geometry of the Model Used.

In the same way as that in the previous work (*Momoi*, 1967a), the breakwater is assumed to be thin plates with infinitesimal thickness, in which two semi-infinite wings run along a single straight line with a small gap. Referring to Fig. 1, the coordinate is centered at the undisturbed water surface at the midpoint of the breakwater gap, of which the

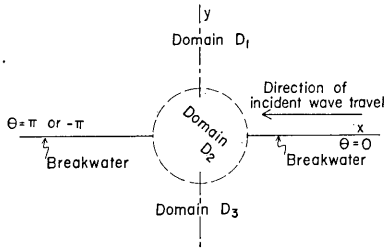

Fig. 1. Geometry of the model used.

breadth is taken as $2d$, the breakwater being situated on the x-axis of the cartesian coordinate. The sea depth is assumed to be uniform throughout the entire domain. Then a train of periodic waves is propagated parallel to the breakwater wings, which is stated by

$$\phi_{in}=\phi_0\, e^{-i\omega t-ikx}\cosh k(z+H)\ , \qquad (1)$$

where

ϕ_{in}: the velocity potential of the incident wave,
ϕ_0: the amplitude of the velocity potential of the incident wave,
H: the depth of the sea,
ω: the angular frequency of the incident wave,
k: the wave number of the incident wave,
t: the time variable,
x and z: the x- and z-components of the cartesian coordinate.

In the above expression, only the real part has a physical meaning.

2,2. Governing Equation and Boundary Conditions.

Assuming irrotational and infinitesimal motion in incompressible water, the velocity potential satisfies the following equation:

$$\left(\frac{\partial^2}{\partial x^2}+\frac{\partial^2}{\partial y^2}+\frac{\partial^2}{\partial z^2}\right)\phi=0\ , \qquad (2)$$

where y is the y-component of the cartesian coordinate, being taken perpendicular to the x-axis through the midpoint of the breakwater gap, and the z-axis is positive upwards.

Let ζ and g be, respectively, the elevation of the water surface and the gravity constant. ζ is expressed as (the relation of energy)

$$\zeta=\frac{1}{g}\left(\frac{\partial\phi}{\partial t}\right)_{z=0}\ . \qquad (3)$$

On the other hand, we have, as a kinematical condition,

$$\frac{\partial\zeta}{\partial t}=-\left(\frac{\partial\phi}{\partial z}\right)_{z=0}\ . \qquad (4)$$

The combination of (3) and (4) yields

$$\frac{\partial^2\phi}{\partial t^2}+g\frac{\partial\phi}{\partial z}=0 \qquad \text{at } z=0\,. \tag{5}$$

The condition at the bottom is given by

$$\frac{\partial\phi}{\partial z}=0 \qquad \text{at } z=-H\,. \tag{6}$$

The boundary condition at the rigid wall of the breakwater is

$$\left.\begin{aligned} &\frac{\partial\phi}{\partial y}=0 \qquad \text{at } (y=0,\ |x|>d)\\ \text{or}\quad &\\ &\frac{\partial\phi}{\partial\theta}=0 \qquad \text{at } (\theta=0 \text{ and } \pi,\ |x|>d)\,. \end{aligned}\right\} \tag{7}$$

In the above, θ is the azimuthal component of the cylindrical coordinate (r, θ, z), r and θ being horizontal and z positive upwards.

Since the incident wave is assumed to be a periodic one, the velocity potential ϕ is expressed as

$$\phi=\phi' e^{-i\omega t}\,, \tag{8}$$

where $e^{-i\omega t}$ is the periodic time factor.

Substituting (8) into the equation (2) and the boundary conditions (5) to (7), these expressions are reduced to :

$$\left(\frac{\partial^2}{\partial x^2}+\frac{\partial^2}{\partial y^2}+\frac{\partial^2}{\partial z^2}\right)\phi'=0\,, \tag{2'}$$

$$\left(-\omega^2+g\frac{\partial}{\partial z}\right)\phi'=0 \qquad \text{at } z=0\,, \tag{5'}$$

$$\frac{\partial\phi'}{\partial z}=0 \qquad \text{at } z=-H\,, \tag{6'}$$

$$\left.\begin{aligned} &\frac{\partial\phi'}{\partial y}=0 \qquad \text{at } (y=0,\ |x|>d)\\ \text{or}\quad &\\ &\frac{\partial\phi'}{\partial\theta}=0 \qquad \text{at } (\theta=0 \text{ and } \pi,\ |x|>d)\,. \end{aligned}\right\} \tag{7'}$$

In the following, the prime ($'$) of ϕ' is omitted as usual, unless otherwise stated.

Under the assumption that the separation of variables is possible, the above equation and the conditions become

$$\left(\frac{\partial^2}{\partial x^2}+\frac{\partial^2}{\partial y^2}+k^2\right)\phi_{xy}=0\ , \tag{9}$$

or

$$\left.\begin{aligned}&\frac{\partial\phi_{xy}}{\partial y}=0 \qquad \text{at } (y=0,\ |x|>d)\\ &\frac{\partial\phi_{xy}}{\partial\theta}=0 \qquad \text{at } (\theta=0 \text{ and } \pi,\ |x|>d)\ ,\end{aligned}\right\} \tag{10}$$

where

$$\phi=\phi_{xy}\cosh k(z+H) \tag{11}$$

and k is an *eigenvalue* of Airy's relation

$$\omega^2=gk\tanh kH\ .$$

In the above, ϕ_{xy} is a function of x and y only.

The incident wave (1) described in complete form is reduced to

$$\left.\begin{aligned}&\phi_{in}=(\phi_{xy})_{in}\cosh k(z+H)\ ,\\ &(\phi_{xy})_{in}=\phi_0\, e^{-ikx}\ ,\end{aligned}\right\} \tag{1'}$$

when the time factor is omitted. The second expression of the above, of course, satisfies equation (9).

2,3. Formal Solution.

In our model (refer to Fig. 1), the portions of the domain are separated into the following three parts, i.e.,

the domain D_1: the region in the range $0<\theta<\pi$ and $d<r$,

the domain D_2: the region in the range $r<d$,

the domain D_3: the region in the range $-\pi<\theta<0$ and $d<r$.

In the above three domains, D_2 is the buffer domain in our method, while D_1 and D_3 are the non-buffer domains.

To begin with, the formal solution in the domain D_1 is given. When a train of the periodic wave expressed by (1') invades the breakwater, the horizontal factor of the velocity potential is described, by use of the first kind of the Hankel function, as follows:

$$\phi_{xy}^{(1)}=\phi_0\, e^{-ikx}+\sum_{m=0}^{\infty}\phi_1^{(m)}H_m^{(1)}(kr)\cos m\theta\ . \tag{12}$$

In the domain D_2, the horizontal factor is expressed by use of the Fourier-Bessel series, i.e.,

$$\phi_{xy}^{(2)}=\sum_{m=0}^{\infty}(\bar{\phi}_2^{(m)}\cos m\theta+\phi_2^{(m)}\sin m\theta)\,J_m(kr)\ . \tag{13}$$

In the domain D_3, the horizontal factor is

$$\phi_{xy}^{(3)}=\sum_{m=0}^{\infty}\phi_3^{(m)}H_m^{(1)}(kr)\cos m\theta\ . \tag{14}$$

In the above expressions, $\phi_{xy}^{(j)}$ $(j=1, 2, 3)$ denote the horizontal factors of the velocity potentials ϕ_j $(j=1, 2, 3)$ in the domains $D_j(j=1, 2, 3)$, which are related by

$$\phi_j=\phi_{xy}^{(j)}\cosh k(z+H) \tag{11'}$$

from (11), and $\phi_1^{(m)}$, $\bar{\phi}_2^{(m)}$, $\phi_2^{(m)}$, $\phi_3^{(m)}$ are the unknown factors to be determined by the boundary conditions between the adjacent domains.

2,4. Conditions between Adjacent Domains.

Since the depth of the sea is assumed to be uniform through the entire domain, the conditions between the adjacent domains are described by use of only the horizontal factors $\phi_{xy}^{(j)}$ $(j=1, 2, 3)$ of the velocity potentials as follows:

$$\left.\begin{aligned}\phi_{xy}^{(2)}&=\phi_{xy}^{(1)}\\ \frac{\partial\phi_{xy}^{(2)}}{\partial r}&=\frac{\partial\phi_{xy}^{(1)}}{\partial r}\end{aligned}\right\}\qquad (r=d,\ 0<\theta<\pi) \tag{15}$$

and

$$\left.\begin{aligned}\phi_{xy}^{(2)}&=\phi_{xy}^{(3)}\\ \frac{\partial\phi_{xy}^{(2)}}{\partial r}&=\frac{\partial\phi_{xy}^{(3)}}{\partial r}\end{aligned}\right\}\qquad (r=d,\ \pi<\theta<2\pi)\ . \tag{16}$$

2,5. Infinite Simultaneous Equations.

Applying the operators

$$\int_0^{\pi}\cos m\theta d\theta\qquad (m=0, 1, 2, \cdots)$$

to (15) after the substitution of (12) and (13) into (15), we have:

$$\begin{aligned}&\bar{\phi}_2^{(2n)}\begin{Bmatrix}J_{2n}(kd)\\ J'_{2n}(kd)\end{Bmatrix}+\frac{2}{\pi}\varepsilon_n\sum_{m=0}^{\infty}\phi_2^{(2m+1)}\frac{2m+1}{(2m+1)^2-(2n)^2}\begin{Bmatrix}J_{2m+1}(kd)\\ J'_{2m+1}(kd)\end{Bmatrix}\\ &\quad=\phi_0\varepsilon_n(-1)^n\begin{Bmatrix}J_{2n}(kd)\\ J'_{2n}(kd)\end{Bmatrix}+\phi_1^{(2n)}\begin{Bmatrix}H_{2n}^{(1)}(kd)\\ H_{2n}^{(1)\prime}(kd)\end{Bmatrix}\qquad (n=0, 1, 2, \cdots)\end{aligned} \tag{17}$$

and

$$\bar{\phi}_2^{(2n+1)}\begin{Bmatrix}J_{2n+1}(kd)\\J'_{2n+1}(kd)\end{Bmatrix}+\frac{4}{\pi}\sum_{m=1}^{\infty}\phi_2^{(2m)}\frac{2m}{(2m)^2-(2n+1)^2}\begin{Bmatrix}J_{2m}(kd)\\J'_{2m}(kd)\end{Bmatrix}$$
$$=i\cdot 2\phi_0(-1)^{n+1}\begin{Bmatrix}J_{2n+1}(kd)\\J'_{2n+1}(kd)\end{Bmatrix}+\phi_1^{(2n+1)}\begin{Bmatrix}H^{(1)}_{2n+1}(kd)\\H^{(1)\prime}_{2n+1}(kd)\end{Bmatrix}\qquad(n=0,1,2,\cdots)\,,\tag{18}$$

where

$$\varepsilon_0=1,\ \varepsilon_n=2\qquad(n\geqq 1)\,,$$

and where the quantities in the wavy brackets are taken in the same order (this convention is followed in the subsequent reductions of the theory, unless otherwise stated). In the above reduction, the incident wave is expanded by use of the formula

$$e^{-ikx}=\sum_{n=0}^{\infty}\varepsilon_n(-1)^n\cos 2n\theta J_{2n}(kr)-i\sum_{n=0}^{\infty}2(-1)^n\cos(2n+1)\theta J_{2n+1}(kr)\,.$$

In like manner, applying the operators

$$\int_{\pi}^{2\pi}\cos m\theta d\theta\qquad(m=0,1,2,\cdots)$$

(the upper and lower limits of the integration differ from those of the fore-going operators) to (16) after the substitution of (13) and (14) into (16), the following equations are obtained:

$$\bar{\phi}_2^{(2n)}\begin{Bmatrix}J_{2n}(kd)\\J'_{2n}(kd)\end{Bmatrix}-\frac{2}{\pi}\varepsilon_n\sum_{m=0}^{\infty}\phi_2^{(2m+1)}\frac{2m+1}{(2m+1)^2-(2n)^2}\begin{Bmatrix}J_{2m+1}(kd)\\J'_{2m+1}(kd)\end{Bmatrix}$$
$$=\phi_3^{(2n)}\begin{Bmatrix}H^{(1)}_{2n}(kd)\\H^{(1)\prime}_{2n}(kd)\end{Bmatrix}\qquad(n=0,1,2,\cdots)\tag{19}$$

and

$$\bar{\phi}_2^{(2n+1)}\begin{Bmatrix}J_{2n+1}(kd)\\J'_{2n+1}(kd)\end{Bmatrix}-\frac{4}{\pi}\sum_{m=1}^{\infty}\phi_2^{(2m)}\frac{2m}{(2m)^2-(2n+1)^2}\begin{Bmatrix}J_{2m}(kd)\\J'_{2m}(kd)\end{Bmatrix}$$
$$=\phi_3^{(2n+1)}\begin{Bmatrix}H^{(1)}_{2n+1}(kd)\\H^{(1)\prime}_{2n+1}(kd)\end{Bmatrix}\qquad(n=0,1,2,\cdots)\,.\tag{20}$$

In the next step, the simplification of the above equations (17)–(20) are made.

Setting

$$\begin{Bmatrix} F_n \\ F'_n \end{Bmatrix} = \frac{2}{\pi}\varepsilon_n \sum_{m=0}^{\infty} \phi_2^{(2m+1)} \frac{2m+1}{(2m+1)^2-(2n)^2} \begin{Bmatrix} J_{2m+1}(kd) \\ J'_{2m+1}(kd) \end{Bmatrix}$$

in the equation (17), we have

$$\bar{\phi}_2^{(2n)} \begin{Bmatrix} J_{2n}(kd) \\ J'_{2n}(kd) \end{Bmatrix} - \phi_1^{(2n)} \begin{Bmatrix} H_{2n}^{(1)}(kd) \\ H_{2n}^{(1)\prime}(kd) \end{Bmatrix}$$
$$= \phi_0 \varepsilon_n (-1)^n \begin{Bmatrix} J_{2n}(kd) \\ J'_{2n}(kd) \end{Bmatrix} - \begin{Bmatrix} F_n \\ F'_n \end{Bmatrix} \qquad (n=0, 1, 2, \cdots) .$$

Solving the above equations in terms of $\bar{\phi}_2^{(2n)}$ and $\phi_1^{(2n)}$, the following are obtained:

$$\bar{\phi}_2^{(2n)} = \phi_0 \varepsilon_n (-1)^n - \frac{1}{\Delta}\{F_n H_{2n}^{(1)\prime}(kd) - F'_n H_{2n}^{(1)}(kd)\} \tag{21}$$

and

$$\phi_1^{(2n)} = \frac{-1}{\Delta}\{F_n J'_{2n}(kd) - F'_n J_{2n}(kd)\} , \tag{22}$$

where

$$\Delta = J_{2n}(kd) H_{2n}^{(1)\prime}(kd) - J'_{2n}(kd) H_{2n}^{(1)}(kd) .$$

In the same way, solving the equations (19) in terms of $\bar{\phi}_2^{(2n)}$ and $\phi_3^{(2n)}$ by use of the notations of F_n and F'_n, we have

$$\bar{\phi}_2^{(2n)} = \frac{1}{\Delta}\{F_n H_{2n}^{(1)\prime}(kd) - F'_n H_{2n}^{(1)}(kd)\} \tag{23}$$

and

$$\phi_3^{(2n)} = \frac{1}{\Delta}\{F_n J'_{2n}(kd) - F'_n J_{2n}(kd)\} . \tag{24}$$

From (21) and (23), $\bar{\phi}_2^{(2n)}$ is reduced to

$$\bar{\phi}_2^{(2n)} = \frac{1}{2}\phi_0 \varepsilon_n (-1)^n . \tag{25}$$

Also, the combination of (22) and (24) yields

$$\phi_1^{(2n)} = -\phi_3^{(2n)} . \tag{26}$$

In like manner, solving the equations (18) in terms of $\bar{\phi}_2^{(2n+1)}$ and $\phi_1^{(2n+1)}$, the solutions

$$\bar{\phi}_2^{(2n+1)} = -i \cdot 2\phi_0(-1)^n + \frac{1}{\chi}\{G_n H_{2n+1}^{(1)\prime}(kd) - G_n' H_{2n+1}^{(1)}(kd)\} \tag{27}$$

and

$$\phi_1^{(2n+1)} = \frac{1}{\chi}\{G_n J_{2n+1}'(kd) - G_n' J_{2n+1}(kd)\} \tag{28}$$

are obtained, where

$$\begin{Bmatrix} G_n \\ G_n' \end{Bmatrix} = \frac{4}{\pi} \sum_{m=1}^{\infty} \phi_2^{(2m)} \frac{2m}{(2m)^2 - (2n+1)^2} \begin{Bmatrix} J_{2m}(kd) \\ J_{2m}'(kd) \end{Bmatrix}$$

and

$$\chi = -J_{2n+1}(kd) H_{2n+1}^{(1)\prime}(kd) + J_{2n+1}'(kd) H_{2n+1}^{(1)}(kd) \ .$$

On the other hand, from the equations (20), $\bar{\phi}_2^{(2n+1)}$ and $\phi_3^{(2n+1)}$ are expressed as (after solving the equations in terms of $\bar{\phi}_2^{(2n+1)}$ and $\phi_3^{(2n+1)}$)

$$\bar{\phi}_2^{(2n+1)} = \frac{-1}{\chi}\{G_n H_{2n+1}^{(1)\prime}(kd) - G_n' H_{2n+1}^{(1)}(kd)\} \tag{29}$$

and

$$\phi_3^{(2n+1)} = \frac{-1}{\chi}\{G_n J_{2n+1}'(kd) - G_n' J_{2n+1}(kd)\} \ . \tag{30}$$

From (27) and (29), $\bar{\phi}_2^{(2n+1)}$ is reduced to

$$\bar{\phi}_2^{(2n+1)} = i\phi_0(-1)^{n+1} \tag{31}$$

and the relation

$$\phi_1^{(2n+1)} = -\phi_3^{(2n+1)} \tag{32}$$

is obtained from (28) and (30).

Substituting (25) into the equations (17), these equations are reduced to

$$\frac{2}{\pi}\varepsilon_n \sum_{m=0}^{\infty} \phi_2^{(2m+1)} \frac{2m+1}{(2m+1)^2 - (2n)^2} \begin{Bmatrix} J_{2m+1}(kd) \\ J_{2m+1}'(kd) \end{Bmatrix} - \phi_1^{(2n)} \begin{Bmatrix} H_{2n}^{(1)}(kd) \\ H_{2n}^{(1)\prime}(kd) \end{Bmatrix}$$
$$= \frac{1}{2}\phi_0 \varepsilon_n (-1)^n \begin{Bmatrix} J_{2n}(kd) \\ J_{2n}'(kd) \end{Bmatrix} \qquad (n = 0, 1, 2, \cdots) \ . \tag{33}$$

Likewise, the substitution of (31) into (18) yields

$$\frac{4}{\pi}\sum_{m=1}^{\infty}\phi_2^{(2m)}\frac{2m}{(2m)^2-(2n+1)^2}\begin{Bmatrix}J_{2m}(kd)\\J'_{2m}(kd)\end{Bmatrix}-\phi_1^{(2n+1)}\begin{Bmatrix}H^{(1)}_{2n+1}(kd)\\H^{(1)\prime}_{2n+1}(kd)\end{Bmatrix}$$

$$=i\phi_0(-1)^{n+1}\begin{Bmatrix}J_{2n+1}(kd)\\J'_{2n+1}(kd)\end{Bmatrix}\qquad(n=0,\,1,\,2,\,\cdots)\,. \tag{34}$$

2,6. Simplified Forms of the Formal Solutions.

Using (25), (26), (31) and (32), the formal expressions (12) to (14) are reduced to the following:

$$\phi_{xy}^{(1)}=\phi_0e^{-ikx}+\phi_{sc}^{(1)}(r,\,\theta_1)\,, \tag{35}$$

$$\phi_{xy}^{(2)}=\frac{1}{2}\phi_0e^{-ikx}+\sum_{m=0}^{\infty}\phi_2^{(m)}\sin m\theta J_m(kr)\,, \tag{36}$$

$$\phi_{xy}^{(3)}=\phi_{xy}^{(3)}(r,\,\theta_3)=-\phi_{xy}^{(1)}(r,\,\theta_1)\,, \tag{37}$$

where

$$\theta_3=-\theta_1\qquad(0<\theta_1<\pi)$$

and

$$\phi_{sc}^{(1)}(r,\,\theta_1)=\sum_{m=0}^{\infty}\phi_1^{(m)}\cos m\theta_1H_m^{(1)}(kr) \tag{38}$$

which is the scattered wave in the windward waters. In the reduction of the expression (36), the formula

$$e^{-ikx}=\sum_{n=0}^{\infty}\varepsilon_n(-1)^n\cos 2n\theta J_{2n}(kr)-i\sum_{n=0}^{\infty}2(-1)^n\cos(2n+1)\theta J_{2n+1}(kr)$$

is employed.

2,7. The $(2l+1)$th Approximation.

Since the equations (33) and (34) are infinite simultaneous equations, these are reduced to a finite number of equations by approximating the expressions of the buffer domain. That is say, setting

$$\left.\begin{aligned}J_m(kr)&\equiv 0\quad(m>2l+1)\\J_m(kr)&\not\equiv 0\quad(m\leqq 2l+1)\end{aligned}\right\}\qquad(l=1,\,2,\,3,\,\cdots)$$

for $r\leqq d$ in (33) and (34), these equations become as follows:

$$\frac{2}{\pi}\varepsilon_n \sum_{m=0}^{l} \phi_2^{(2m+1)} \frac{2m+1}{(2m+1)^2-(2n)^2} \begin{Bmatrix} J_{2m+1}(kd) \\ J'_{2m+1}(kd) \end{Bmatrix} - \phi_1^{(2n)} \begin{Bmatrix} H_{2n}^{(1)}(kd) \\ H_{2n}^{(1)\prime}(kd) \end{Bmatrix}$$

$$= \frac{1}{2}\phi_0 \varepsilon_n (-1)^n \begin{Bmatrix} J_{2n}(kd) \\ J'_{2n}(kd) \end{Bmatrix} \qquad (n=0, 1, 2, \cdots, l) , \tag{39}$$

$$\frac{2}{\pi}\varepsilon_n \sum_{m=0}^{l} \phi_2^{(2m+1)} \frac{2m+1}{(2m+1)^2-(2n)^2} J_{2m+1}(kd) - i\phi_1^{(2n)} Y_{2n}(kd)$$

$$= 0 \qquad (n=l+1, l+2, \cdots) , \tag{40}$$

$$\frac{4}{\pi} \sum_{m=1}^{l} \phi_2^{(2m)} \frac{2m}{(2m)^2-(2n+1)^2} \begin{Bmatrix} J_{2m}(kd) \\ J'_{2m}(kd) \end{Bmatrix} - \phi_1^{(2n+1)} \begin{Bmatrix} H_{2n+1}^{(1)}(kd) \\ H_{2n+1}^{(1)\prime}(kd) \end{Bmatrix}$$

$$= i\phi_0 (-1)^{n+1} \begin{Bmatrix} J_{2n+1}(kd) \\ J'_{2n+1}(kd) \end{Bmatrix} \qquad (n=0, 1, 2, \cdots, l-1) , \tag{41}$$

$$\frac{4}{\pi} \sum_{m=1}^{l} \phi_2^{(2m)} \frac{2m}{(2m)^2-(2n+1)^2} J_{2m}(kd) + i\phi_0 (-1)^n \mu_n J_{2n+1}(kd)$$

$$= \phi_1^{(2n+1)} \{\mu_n J_{2n+1}(kd) + i Y_{2n+1}(kd)\} \qquad (n=l, l+1, \cdots) , \tag{42}$$

where

$$\mu_n = 1 \qquad \text{for} \quad n=l ,$$
$$\mu_n = 0 \qquad \text{for} \quad n \geqq l+1 .$$

In the above equations, the first two ((39) and (40)) are derived from (33), while the second two ((41) and (42)) are obtained from (34). As already mentioned, the quantities in the wavy brackets are taken in the same order.

Now, if one specifies the value of l or the degree of the approximation, the unknowns

$$\phi_2^{(2n+1)} \text{ and } \phi_1^{(2n)} \qquad (n=0, 1, 2, \cdots, l)$$

are readily calculated from the finite simultaneous equations (39), the higher modes

$$\phi_1^{(2n)} \qquad (n=l+1, l+2, \cdots)$$

being obtained by the substitution of $\phi_2^{(2n+1)}$ $(n=0, 1, 2, \cdots, l)$ into (40).

In like manner, the unknowns

$$\phi_2^{(2m)} \text{ and } \phi_1^{(2n-1)} \qquad (m=1, 2, \cdots, l;\ n=0, 1, \cdots, l-1)$$

are calculated by the equations (41), the higher modes

$$\phi_1^{(2n+1)} \qquad (n=l, l+1, \cdots)$$

being computed by the substitution of $\phi_2^{(2m)}$ $(m=1, 2, \cdots, l)$ into (42).

Using the unknown factors obtained in such a way, the behavior of the waves around the gap of the breakwater wings can be discussed through the formal expressions (35) to (38). The actual calculations of the above mentioned procedures are carried out with the aid of an electronic computer.

In the case of the present paper, the depth of water is assumed to be uniform throughout the entire domain. The relation of the wave height ζ and the velocity potential ϕ is given by

$$\frac{\zeta}{\zeta_0}=\frac{\phi}{\phi_0} \tag{43}$$

where ζ_0 is referred to the wave height of the incident wave. For the reduction of the above relation, the reader should refer to Section *2,9* of the previous work (*Momoi*, 1967b).

3. Numerical Calculations and Discussions

Following the procedures mentioned in the previous section, numerical calculations are carried out. The calculated ranges are $kd=0.01$ to 0.2 for the phase variation of the wave in the windward waters and $kd=0.1$ to 3.0 for the amplitude and phase variations in the entire domain of waters. The former of the variations are depicted in Figs. 2a (or 2b) to 8a (or 8b), where two figures are arranged for each kd in order to avoid any misunderstanding of the calculated result due to the employed approximation. The latter are described in Figs. 10 to 14.

3,1. Appearance of Reverse Current

To begin with, the phase variations of the windward waters are discussed for the range $kd=0.01$ to 0.2. Through Figs. 2a (or 2b) to 8a (or 8b), most conspicuous feature is the appearance of the waves (reverse current) converging toward the nearby waters of the leeward terminus of the breakwater wings (see Fig. 9). When the wave-length of the incident wave is very long compared with the width of the breakwater gap (refer to Figs. 2a (or 2b) to 4a (or 4b)), the above reverse current is so strong that a nearly circular current toward the breakwater gap is found, while, when the wave-length becomes relatively small (refer to Figs. 5a (or 5b) to 7a (or 7b)), the reverse current becomes gradually weaker until little converging wave is found (see Figs. 8a (or

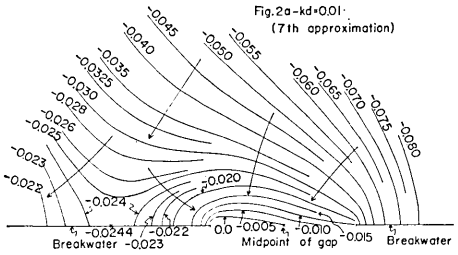

Fig. 2a. Phase variation of the wave in the windward waters for $kd=0.01$ under the seventh approximation (the following thirteen figures 2b, 3a, 3b, 4a, 4b, 5a, 5b, 6a, 6b, 7a, 7b, 8a, and 8b show the phase variations of the wave in the windward waters).

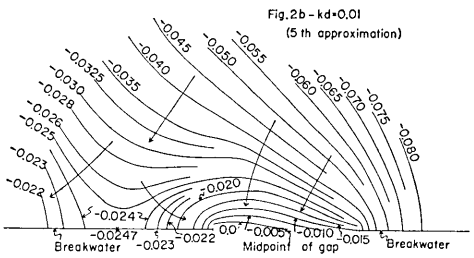

Fig. 2b. Phase variation for $kd=0.01$ under the fifth approximation.

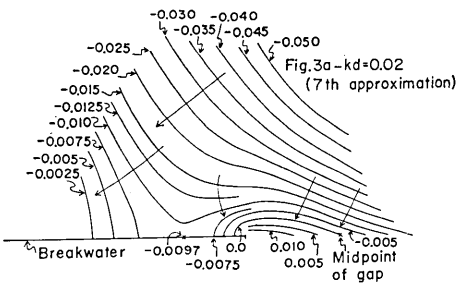

Fig. 3a. Phase variation for $kd=0.02$ under the seventh approximation.

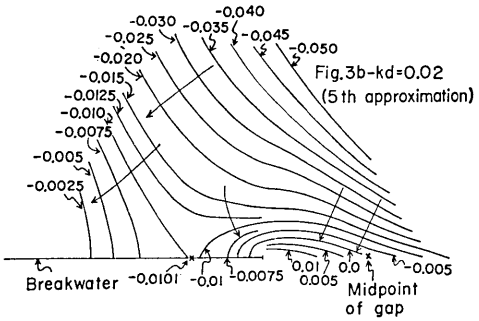

Fig. 3b. Phase variation for $kd=0.02$ under the fifth approximation.

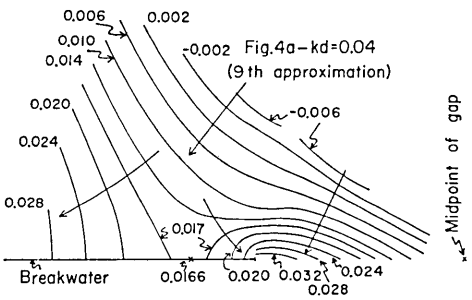

Fig. 4a. Phase variation for $kd=0.04$ under the ninth approximation.

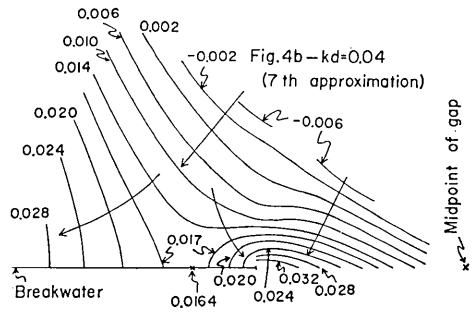

Fig. 4b. Phase variation of the wave for $kd=0.04$ under the seventh approximation.

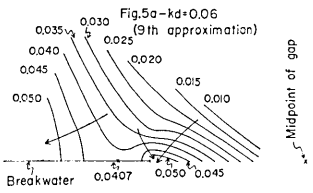

Fig. 5a. Phase variation for $kd=0.06$ under the ninth approximation.

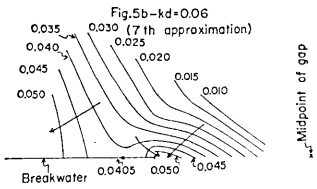

Fig. 5b. Phase variation for $kd=0.06$ under the seventh approximation.

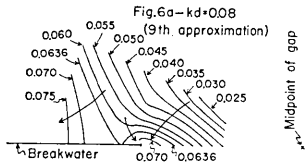

Fig. 6a. Phase variation for $kd=0.08$ under the ninth approximation.

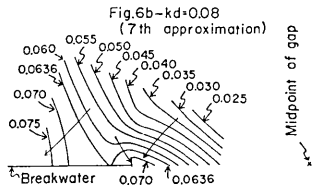

Fig. 6b. Phase variation for $kd=0.08$ under the seventh approximation.

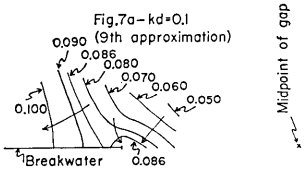

Fig. 7a. Phase variation for $kd=0.1$ under the ninth approximation.

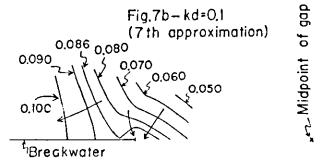

Fig. 7b. Phase variation for $kd=0.1$ under the seventh approximation.

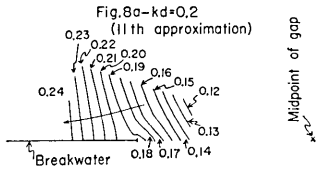

Fig. 8a. Phase variation for $kd=0.2$ under the eleventh approximation.

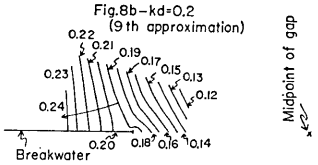

Fig. 8b. Phase variation for $kd=0.2$ under the ninth approximation.

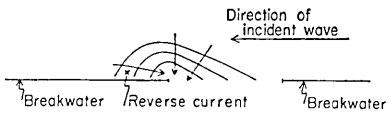

Fig. 9. Appearance of the converging wave (reverse current) around the leeward terminus of the breakwater wing.

8b)). The above strong reverse current for the very long wave is due to the strong diffraction of the long wave and, as kd increases, the diffraction becomes gradually weaker.

3,2. Amplitude and Phase Variations throughout the Entire Domain.

The amplitude and phase variations of the RST (resultant) wave are discussed for the waves in the range $kd=0.1$ to 3.0, which are depicted in Figs. 10cw (cl, aw, pw, al or pl) to 14cw (cl, aw, pw, al or pl)*. The subscript cw and cl denote, respectively, the figures relevant to the convergence check of the approximated theory in the windward and leeward waters. The subscript aw and pw refer to the figures concerning the overall variations of the amplitude and phase in the windward waters, while al and pl denote those in the leeward waters.

Before proceeding with the discussion of the overall variations of the amplitude and phase, the convergence check is made for the amplitudes in the typical directions, i.e., $\theta=0\pm\varepsilon$, $\pm\pi/2$ and $\pm\pi$ (ε: an infinitesimal). According to Figs. 10cw (cl) to 14cw (cl), the agreements of the curves of the stated approximations are found to be fairly good except for the part near $r/d=1.0$, in which slight disagreements are found. In drafting the pictures showing the overall variations of the amplitude and phase, these disagreements are smoothed out by hand. In the curves of the amplitude along the windward side of the breakwater wall (the curves of $\theta=0+\varepsilon$ in Figs. 12cw, 13cw, and 14cw except 10cw and 11cw), the undulatory variations having $|\zeta/\zeta_0|=1.0$ as the axis of the undulation are found, among which the first undulation is the greatest in amplitude. Comparing the scale of the wave-length λ of the incident

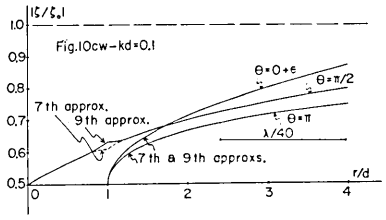

Fig. 10cw. Convergence check of the approximated theory in the windward waters for $kd=0.1$.

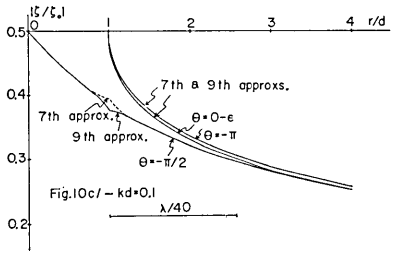

Fig. 10cl. Convergence check of the approximated theory in the leeward waters for $kd=0.1$.

*) The approximations employed in drafting these pictures are the 9th approximation for Fig. 10 ($kd=0.1$), the 13th approximation for Fig. 11 ($kd=0.5$), the 17th approximation for Fig. 12 ($kd=1.0$), the 21st approximation for Fig. 13 ($kd=2.0$) and the 23rd approximation for Fig. 14 ($kd=3.0$).

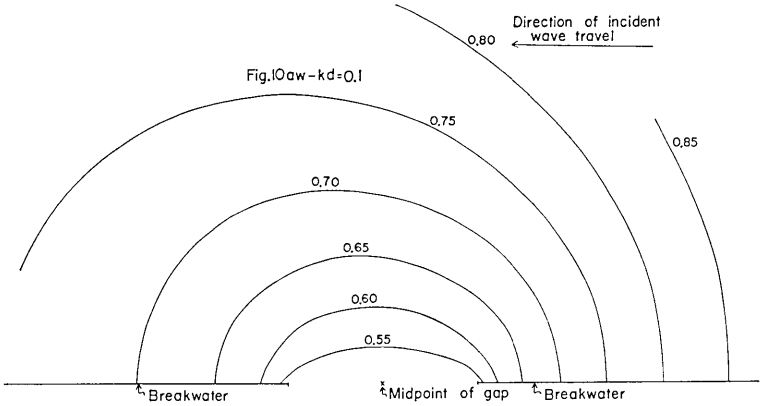

Fig. 10aw. Overall variation of amplitude in the windward waters for $kd=0.1$. The stated values in the figure denote $|\zeta/\zeta_0|$.

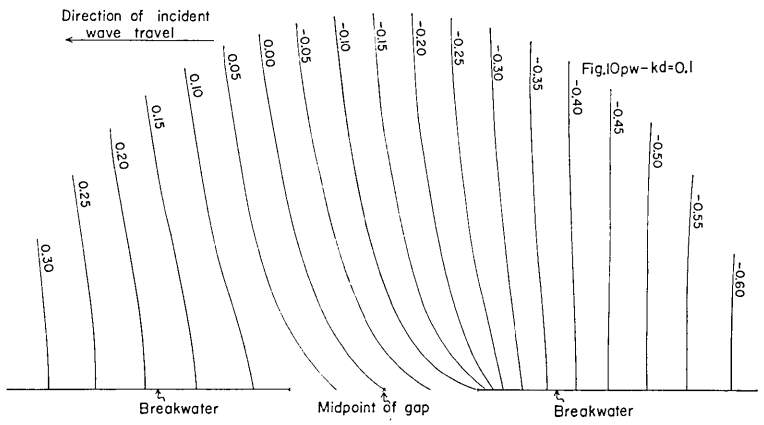

Fig. 10pw. Overall variation of phase in the windward waters for $kd=0.1$. The stated values in the figure denote arg ζ.

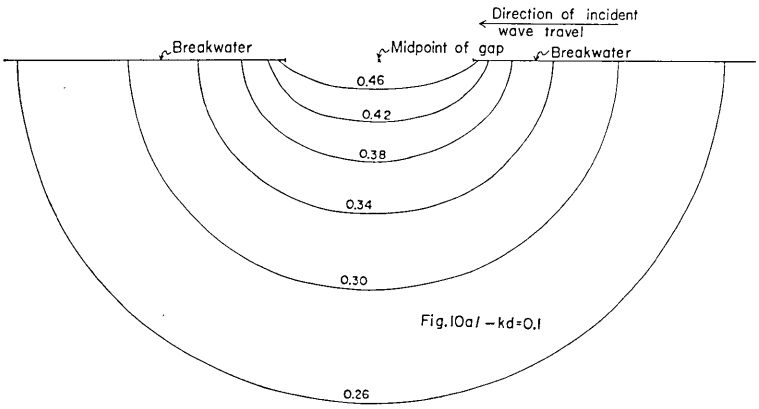

Fig. 10a*l*. Overall variation of amplitude in the leeward waters for $kd=0.1$. The stated values in the figure denote $|\zeta/\zeta_0|$.

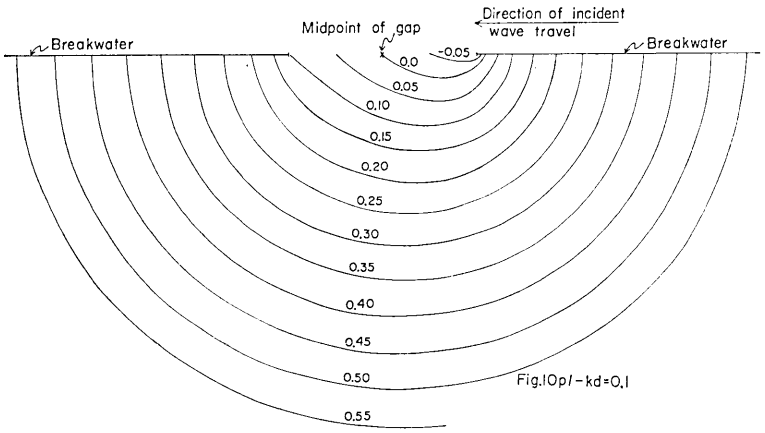

Fig. 10p*l*. Overall variation of phase in the leeward waters for $kd=0.1$. The stated values in the figure denote arg ζ.

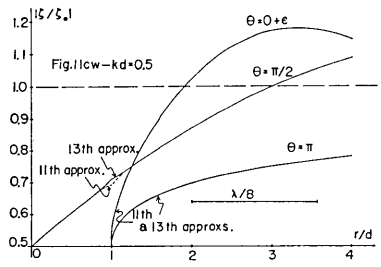

Fig. 11cw. Convergence check of the approximated theory in the windward waters for $kd=0.5$.

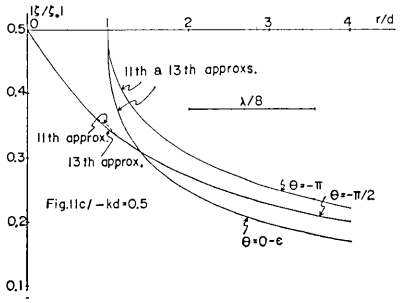

Fig. 11c*l*. Convergence check of the approximated theory in the leeward waters for $kd=0.5$.

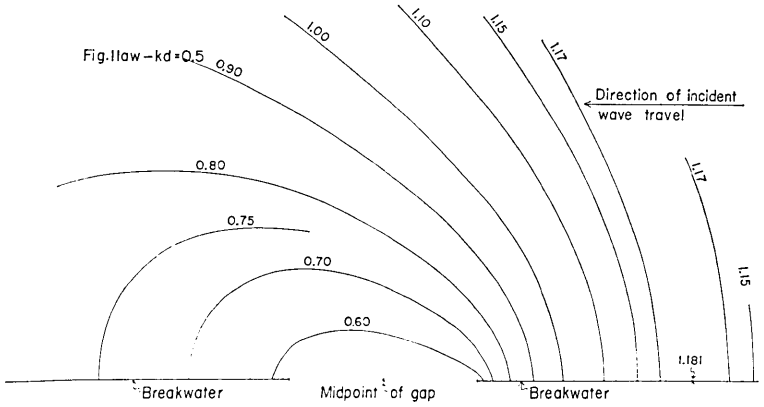

Fig. 11aw. Overall variation of amplitude in the windward waters for $kd=0.5$. The stated values in the figure denote $|\zeta/\zeta_0|$.

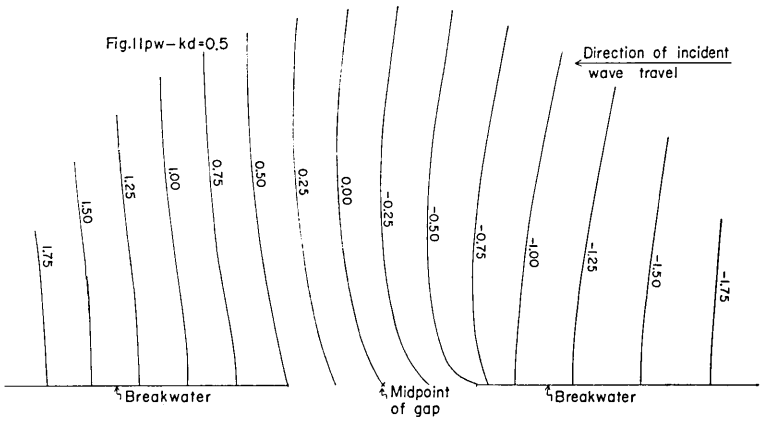

Fig. 11pw. Overall variation of phase in the windward waters for $kd=0.5$. The stated values in the figure denote $\arg \zeta$.

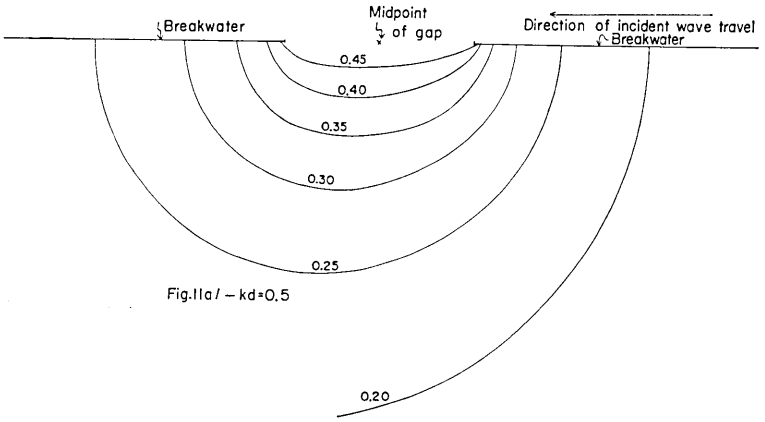

Fig. 11a*l*. Overall variation of amplitude in the leeward waters for $kd=0.5$. The stated values in the figure denote $|\zeta/\zeta_0|$.

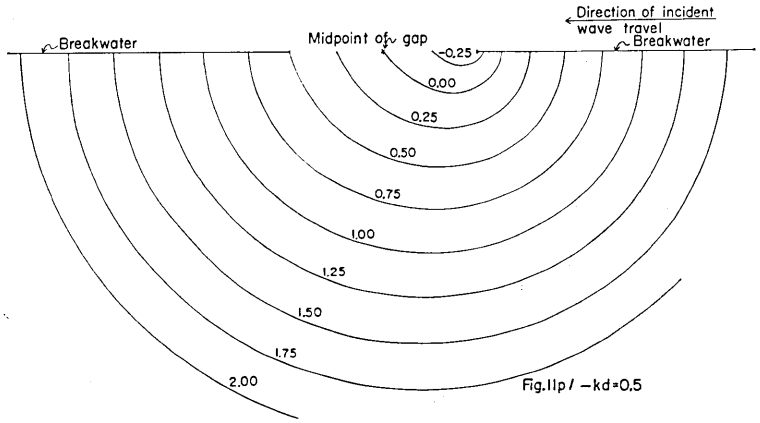

Fig. 11p*l*. Overall variation of phase in the leeward waters for $kd=0.5$. The stated values in the figure denote $\arg \zeta$.

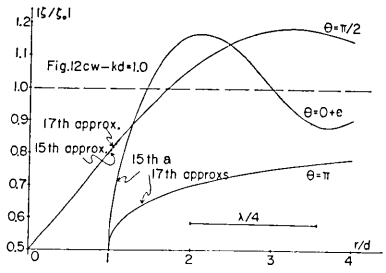

Fig. 12cw. Convergence check of the approximated theory in the windward waters for $kd=1.0$.

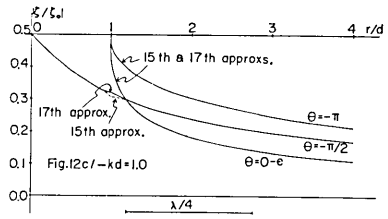

Fig. 12*cl*. Convergence check of the approximated theory in the leeward waters for $kd=1.0$.

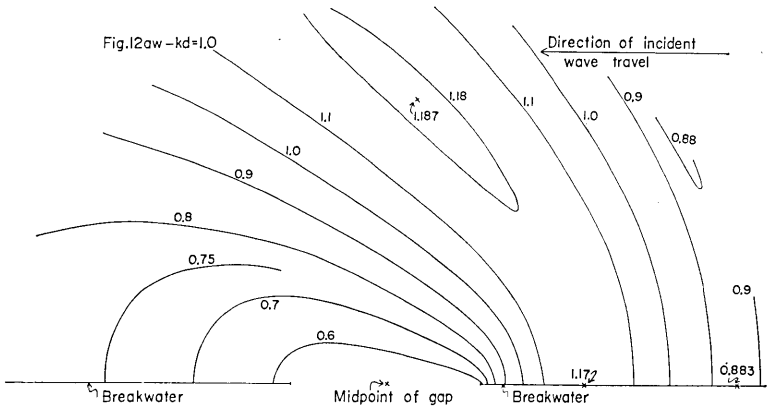

Fig. 12aw. Overall variation of amplitude in the windward waters for $kd=1.0$. The stated values in the figure denote $|\zeta/\zeta_0|$.

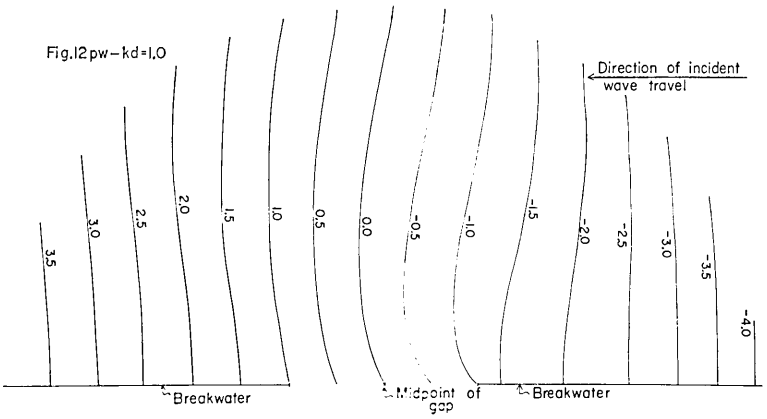

Fig. 12pw. Overall variation of phase in the windward waters for $kd=1.0$. The stated values in the figure denote arg ζ.

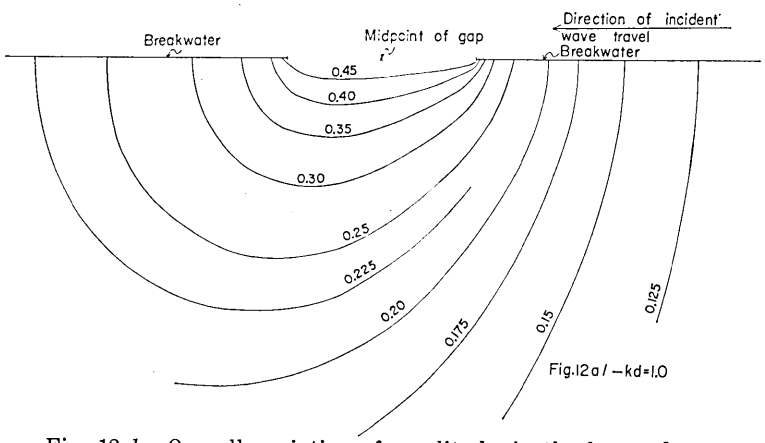

Fig. 12a*l*. Overall variation of amplitude in the leeward waters for $kd=1.0$. The stated values in the figure denote $|\zeta/\zeta_0|$.

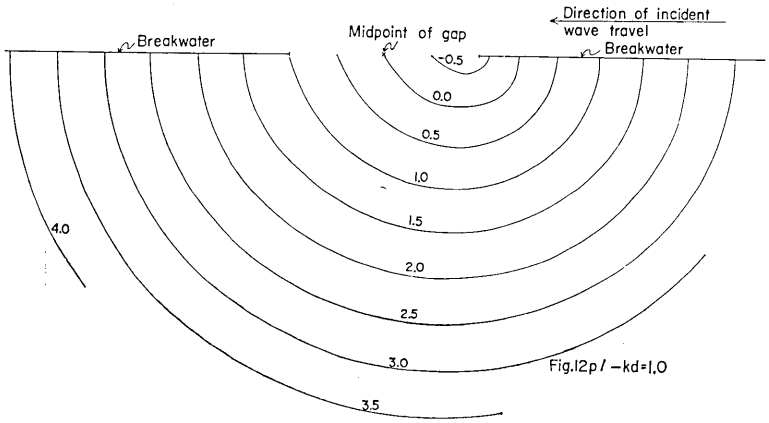

Fig. 12p*l*. Overall variation of phase in the leeward waters for $kd=1.0$. The stated values in the figure denote $\arg\zeta$.

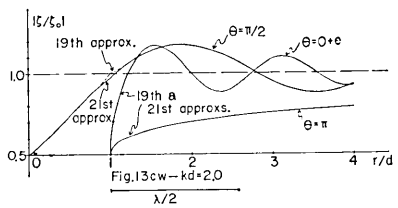

Fig. 13c*w*. Convergence check of the approximated theory in the windward waters for $kd=2.0$.

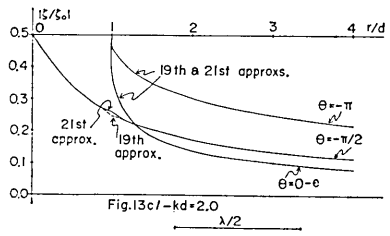

Fig. 13c*l*. Convergence check of the approximated theory in the leeward waters for $kd=2.0$.

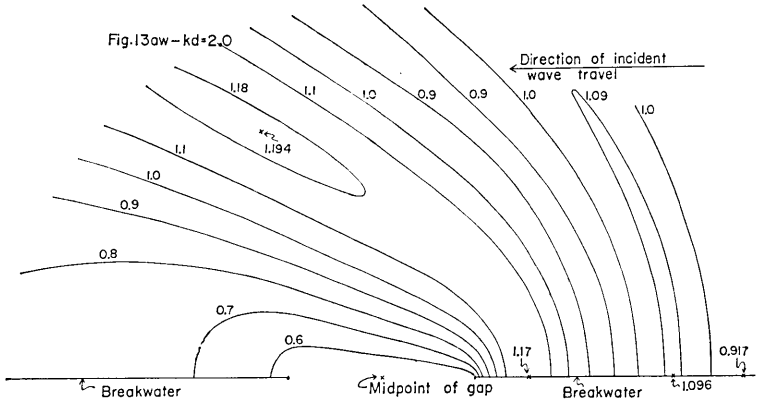

Fig. 13aw. Overall variation of amplitude in the windward waters for $kd=2.0$. The stated values in the figure denote $|\zeta/\zeta_0|$.

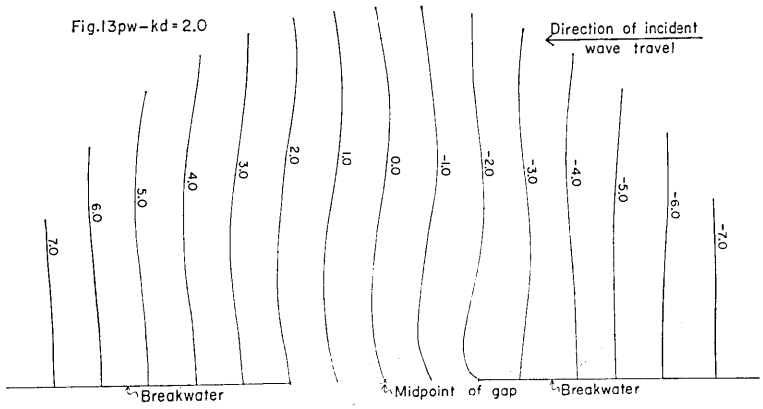

Fig. 13pw. Overall variation of phase in the windward waters for $kd=2.0$. The stated values in the figure denote arg ζ.

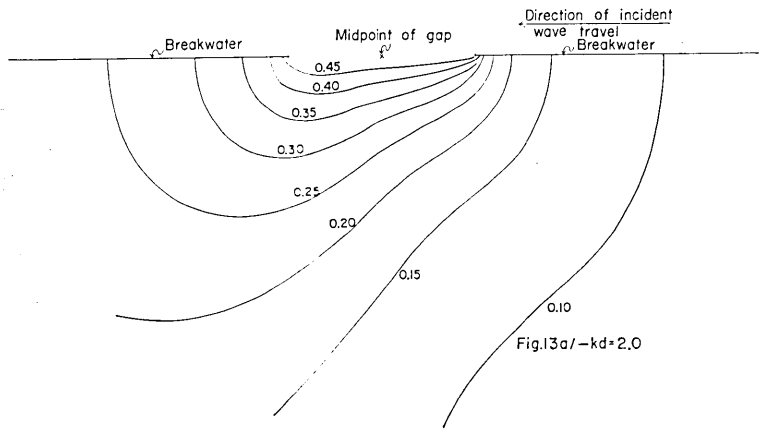

Fig. 13a*l*. Overall variation of amplitude in the leeward waters for $kd=2.0$. The stated values in the figure denote $|\zeta/\zeta_0|$.

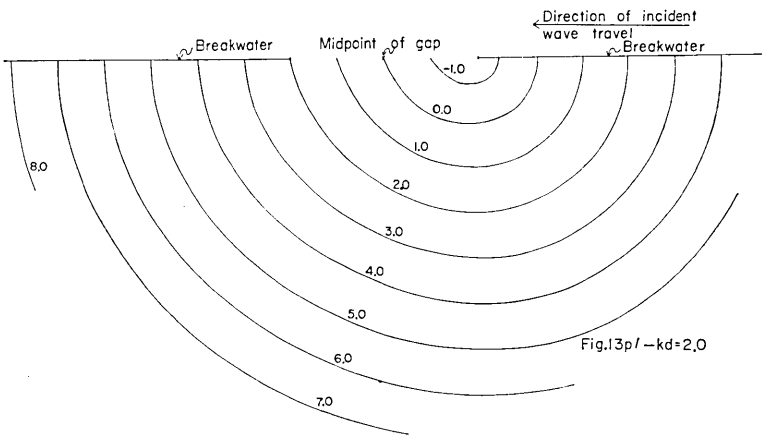

Fig. 13p*l*. Overall variation of phase in the leeward waters for $kd=2.0$. The stated values in the figure denote $\arg\zeta$.

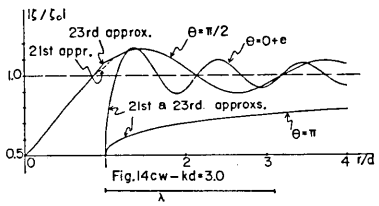

Fig. 14cw. Convergence check of the approximated theory in the windward waters for $kd=3.0$.

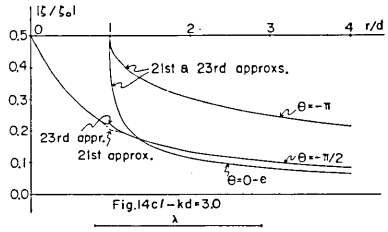

Fig. 14c*l*. Convergence check of the approximated theory in the leeward waters for $kd=3.0$.

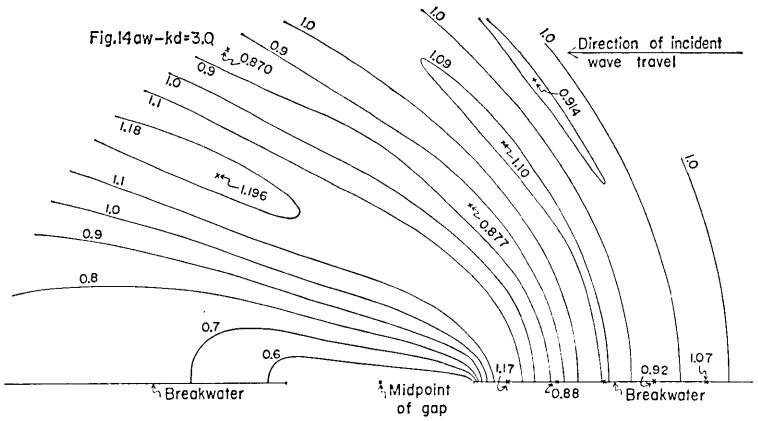

Fig. 14aw. Overall variation of amplitude in the windward waters for $kd=3.0$. The stated values in the figure denote $|\zeta/\zeta_0|$.

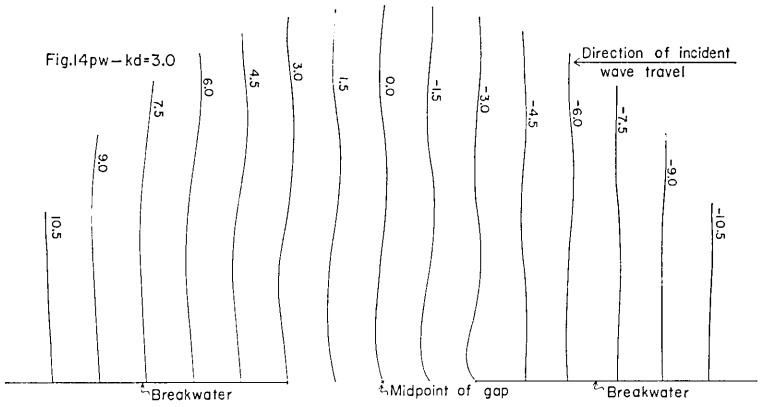

Fig. 14pw. Overall variation of phase in the windward waters for $kd=3.0$. The stated values in the figure denote $\arg\zeta$.

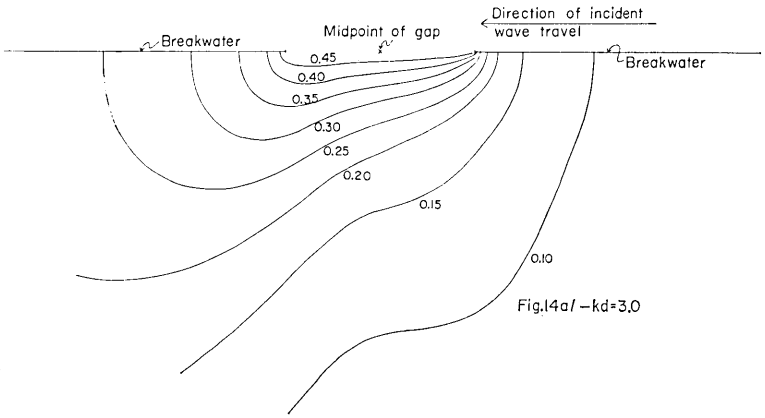

Fig. 14a*l*. Overall variation of amplitude in the leeward waters for $kd=3.0$. The stated values in the figure denote $|\zeta/\zeta_0|$.

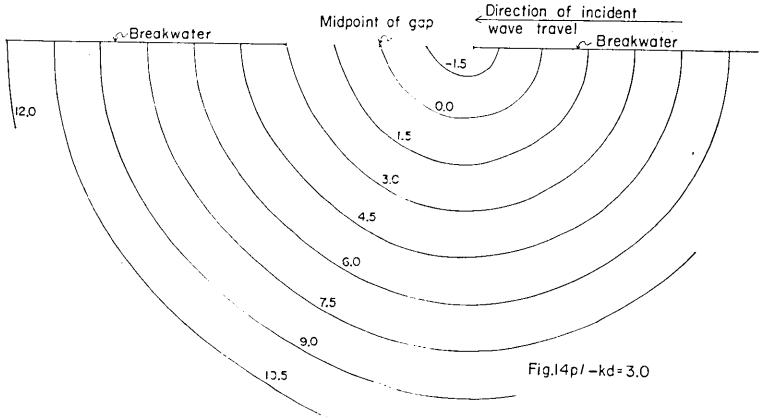

Fig. 14p*l*. Overall variation of phase in the leeward waters for $kd=3.0$. The stated values in the figure denote $\arg\zeta$.

wave (drawn in each figure for Figs. 10cw to 14cw) and the undulatory variation of the amplitude, these undulations are found to be repeated with a half wave-length of the incident wave ($\lambda/2$) in the direction $\theta=0+\varepsilon$ and with the wave-length (λ) in the direction $\theta=\pi/2$. On the other hand, the amplitude in the direction $\theta=\pi$ increases monotonically other than those in the directions $\theta=0+\varepsilon$ and $\pi/2$ (Fig. 15). Inspection of Figs. 10c*l* to 14c*l* (the figures concerning the variation of the amplitude in the typical directions of the leeward waters) shows that the directivity of the wave transmitted through the breakwater gap becomes more and more definite as kd increases. When $kd=0.1$ (Fig. 10c*l*), the difference of the curves in the three directions is very slight due to the strong diffraction of the wave, while, when kd becomes 2.0 or 3.0 (Fig. 13c*l* or 14c*l*), the wave in the direction $\theta=-\pi$ is in amplitude nearly twice those in the directions $\theta=0-\varepsilon$ and $-\pi/2$.

Now, let us discuss the overall variations of the amplitude and phase around the breakwater gap.

To begin with, the amplitude variations in the windward waters are illustrated, which are shown, respectively, in Figs. 10aw, 11aw, 12aw, 13aw and 14aw for $kd=0.1, 0.5, 1.0, 2.0$ and 3.0. When kd is small (say the cases of Figs. 10aw and 11aw), the contours of the amplitude take a circular form. As kd increases (say Figs. 12aw to 14aw), the region of low amplitude begins to extend along the breakwater wing on the leeward side owing to the growing nature of the directivity of waves (see Fig. 16).

Referring to the figures relevant to the phase variation in the windward waters (Figs. 10pw, 11pw, 12pw, 13pw and 14pw for $kd=0.1$, 0.5, 1.0, 2.0 and 3.0 respectively), the following are found. The wave is propagated, as a general trend, from the right (windward side) to the left (leeward side). When $kd=0.1$ (Fig. 10pw), the component of the wave advancing toward the breakwater gap is great, becoming gradually smaller

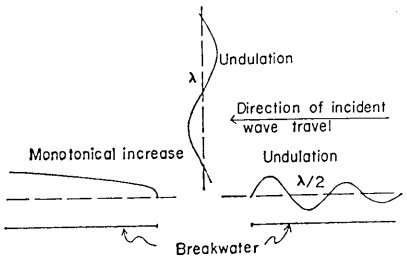

Fig. 15. Amplitude variations in the typical directions of the windward waters.

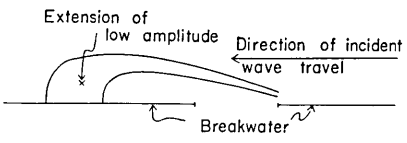

Fig. 16. Extension of low amplitude area along the forward part of the breakwater of the leeward side.

with the increase of kd (Figs. 11pw to 14pw). In the nearby waters of the terminus of the windward breakwater, a sudden change of the contour of the phase appears, which is interpreted as being due to the hair-pin bend of the wave toward the leeward waters (see Fig. 17).

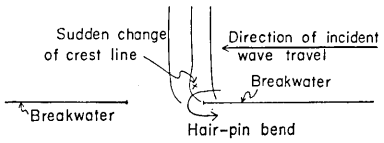

Fig. 17. Appearance of the sudden change of the crest line near the windward terminus of the breakwater.

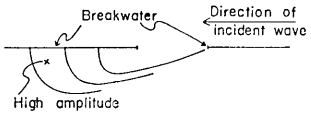

Fig. 18. Extension of the high amplitude region along the backward part of the breakwater of the leeward side.

According to Figs. 10al to 14al (the figures concerning the amplitude variation in the leeward waters), the contours of the amplitude form a circular pattern for small kd (say Fig. 10al or 11al), showing the gradual extension of the high amplitude region along the breakwater wing on the leeward side (see Fig. 18) with the increase of kd (say Figs. 12al to 14al).

Finally, mention is made of the phase variations in the leeward waters (refer to Figs. 10pl to 14pl). Passing through Figs. 10pl to 14pl, the waves invading through the breakwater gap start from the terminus of the windward breakwater (see Fig. 19). The waves near the gap are propagated in the direction away from that of the incident wave travel for $kd=0.1$ or 0.5 (Fig. 10pl or 11pl), while the above travelling sense of the wave is directed toward the leeward of the incident wave with

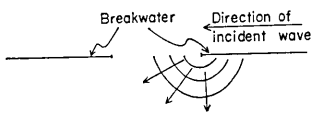

Fig. 19. Emission of the wave from the terminus of the windward breakwater toward the backward waters.

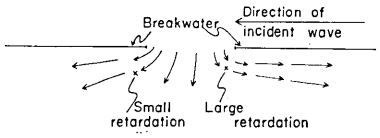

Fig. 20. Phase retardation of the wave around the termini of the breakwater.

the augmentation of kd (Figs. 12pl to 14pl). When kd is small (say Fig. 10pl), the waves turning in the waters near the two terminuses of the breakwater are retarded. The retardation of the wave near the windward terminus is then greater than that near the leeward terminus (refer to Fig. 20). When kd becomes large, the above retardation gradually disappears (refer to Figs. 11pl to 14pl).

References

MOMOI, T., 1967a, A Long Wave around a Breakwater (Case of Perpendicular Incidence) [I], *Bull. Earthq. Res. Inst.*, **45**, 91-136.

MOMOI, T., 1967b, A Long Wave around a Breakwater (Case of Perpendicular Incidence) [II], *Bull Earthq. Res. Inst.*, **45**, 749-783.

MOMOI, T., 1967c, A Long Wave around a Breakwater (Case of Perpendicular Incidence) [III], *Bull. Earthq. Res. Inst.*, **46**, 125-135.

MORSE, P. M. and RUBENSTEIN, P. J., 1938, The diffraction of waves by ribbons and by slits, *Physical Review*, **54**, 895-898.

14. 防波堤のまわりにおける長波 (横入射の場合) [IV]

地震研究所　桃井高夫

本論説においては，入射波が防波堤にそつて進入する場合について，防波堤の開口部近傍における長波の状態が論じられている．得られた結論のうち最も顕著なのは，非常に長い波について風下側の防波堤開口端の近くに入射波の方向とは反対向きの逆流がおきることである．